Supporting information

Boosting OER performance of IrO_2 in acid via urchinlike hierarchical-structure design

Qian Deng[1,2†], You Sun[2†], Jin Wang[1,2†*], Shengding Chang[2], Muwei Ji[2,3], Yunteng Qu[4], Kai Zhang[2] and Bo Li[2*]

[1] College of Materials Science and Engineering, Shenzhen University, Shenzhen 518060, China
[2] Tsinghua Shenzhen International Graduate School, Tsinghua University, Shenzhen 518055, China
[3] College of Chemistry and Environmental Engineering, Shenzhen University, Shenzhen 518060, China
[4] Department of Chemistry, Hefei National Laboratory for Physical Sciences at the Microscale, iChEM (Collaborative Innovation Center of Chemistry for Energy Materials), University of Science and Technology of China, Hefei 230026, China

[†] These authors contributed equally to this study.
[*] Corresponding authors (emails: wangjin19@szu.edu.cn (Wang J); boli@mail.tsinghua.edu.cn (Li B))

Experimental Section

Synthesis of iridium oxide samples

Iridium oxide nanoparticles with different morphology were synthesized by two-step hydrothermal method. 0.03 g $IrCl_3$ (99.8 wt%, Alfa Aesar) was dissolved in 15 mL deionized water, and then 1 mL 30 % H_2O_2 was added to the solution. The aqueous solution was stirred at 100 ℃ for 3 h. Then 5 mL 2 M NaOH solution was added and a purple suspension was formed. 20 mL as-prepared feedstock was filled in a 25 mL autoclave and subjected to heat treatment at different temperatures varying from 160 ℃ to 200 ℃ for different duration. The final product was obtained after washing with deionized water and centrifuging for several cycles and dried at 50 ℃.

Electrochemical measurements

Electrochemical measurements were carried out at 25 ℃ in a typical three-electrode glass cell connected with the electrochemical workstation (CHI 760E). The electrolyte was 0.5 M H_2SO_4 solution. The reference electrode was Ag/AgCl electrode and the counter electrode was platinum electrode. The rotating speed was 1600 r/min.

The working electrode was 5 mm in diameter corresponding to a geometric surface area of 0.196 cm^2 and were mounted in a rotating disk. The catalysts ink was prepared as follows: firstly, 5

mg of the catalyst were dispersed in a solution containing 600 μL isopropanol, 384 μL deionized water and 16 μL Nafion solution (5 wt%, Aldrich). Then 10 μL mixture was dropped on the surface of the working electrode to achieve a loading of 0.26 mg cm^{-2}.

The working electrodes were prepared by two method. When conducting LSV, CV, EIS tests, the working electrode were prepared by dropping the above catalysts ink on glassy carbon disk. As the catalyst tend to peel off from the smooth surface of the glassy carbon disk during long-time measurement (Fig. S5), the catalyst ink was dropped on sticky carbon (Fig. S9) for CP measurement. The sticky carbon was prepared by blending eicosane with carbon black in a mass ratio of 5:1 at 50 °C. The sticky carbon was then filled into an empty well of a rotating disk electrode (5 mm in diameter) under irradiation of an infrared lamp to form a relatively smooth surface, and then was solidified at room temperature. Then 10 μL mixture of catalyst ink was dropped on the surface of the prepared sticky carbon.

The electrochemical surface active area (ECSA) of the IrO_2 samples were estimated from double layer capacitance(C_{dl}) and specific capacitance(C_s) using the following equation.

$$ECSA\ (m^2 g^{-1}) = \frac{C_{dl}}{C_s \times m}$$

Where, C_{dl} is the measured double-layer capacitance (mF) from the CV curves in the non-faradaic region (Fig. S4), m is mass loading of the electrocatalyst (g) and C_s is the specific capacitance of the sample or the capacitance of an atomically smooth planar surface of the material per unit area under identical electrolyte conditions. For our estimates of electrochemical specific surface area, we used general specific capacitances of $C_s = 0.035$ mF cm^{-2} in 0.5M H_2SO_4 based on typically reported value [1].

The calculation of the charge transfer resistance from the Nyquist plot:

To determine the solution resistance (R_s), electrode resistance (R_1) and the surface charge transfer resistance (R_{ct}) of the as-prepared IrO_2, EIS has been performed. The EIS was performed in the frequency range of 0.01-10000 Hz using the electrochemical work station (CHI 760E) in 0.5 M H_2SO_4 electrolyte solution at 25 °C under a constant voltage of 1.45 V (vs RHE).

In inset of Fig. 4 (a), the fitting of an $R_s(R_1CPE_1)(R_{ct}CPE_2)$ circuit for OER at an anodic IrO_2 electrode is presented. This circuit is identical to the one proposed by Lasia and co-workers for

hydrogen evolution at porous Ni electrodes [2, 3] and by Trasatti and co-workers for oxygen evolution at porous IrO_2-based electrodes [4]. In this model, the first Randles-type circuit describes ionic migration phenomena within the pores of the electrode (dominant at high frequencies) whereas the second one describes the charge transfer at the electrode.

The Z-View software from Scribner Associates employing the $R_s(R_1CPE_1)(R_{ct}CPE_2)$ equivalent circuit was used to model the impedance data for OER. After fitting the circuit in Z-view, the R_s values of IrO_2-160, IrO_2-180 and IrO_2-200 are 5.78 Ω, 4.90 Ω and 5.70 Ω, respectively. The resistance is almost the same because the electrolyte is H_2SO_4 solution. The R_{ct} of IrO_2-180 is only 169.5 Ω, which is much smaller than 496.4 Ω of IrO_2-160 and 421.2 Ω of IrO_2-200, indicating that the resistance of charge transfer process is smaller and the catalytic reaction kinetics is faster.

Figures

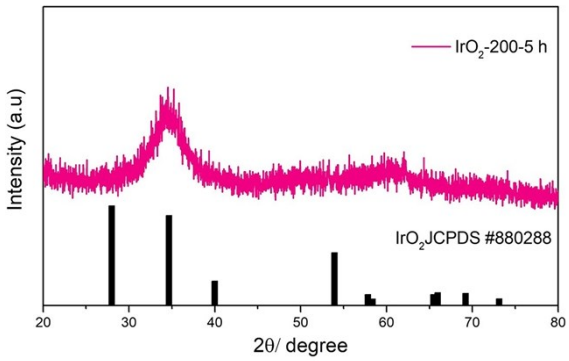

Fig. S1 The XRD pattern of the product after hydrothermal treatment at 200℃ for 5 h (IrO_2-200-5 h)

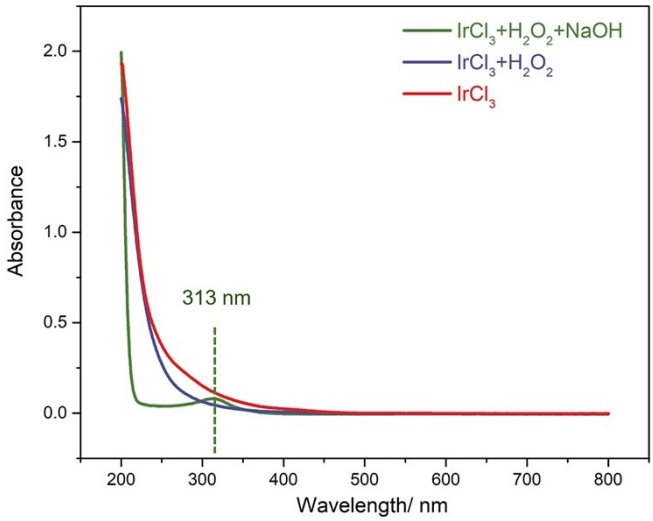

Fig. S2 UV-Vis spectra of the Ir-precursors in the feedstocks derived with different recipes.

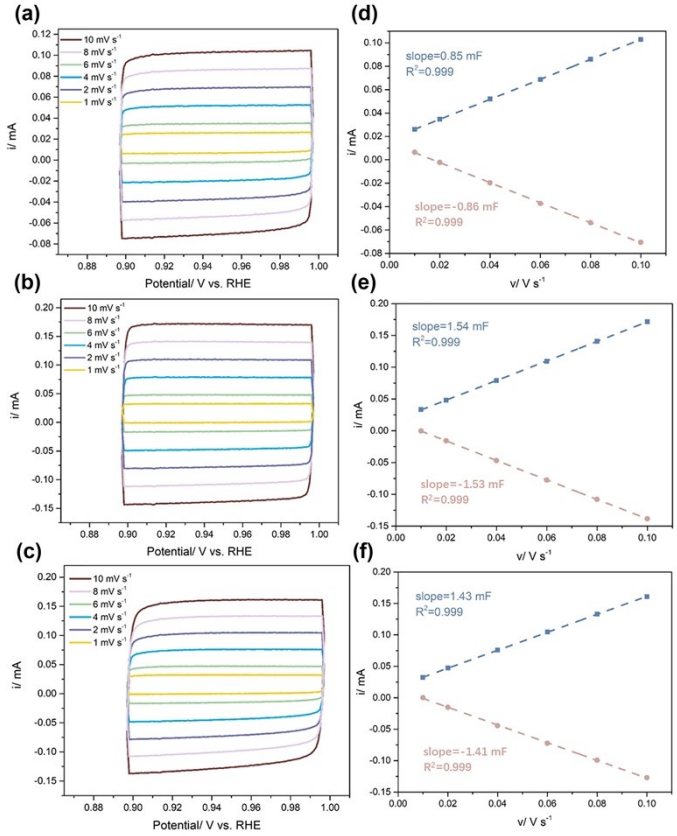

Fig. S3 Double layer capacitance (C_{dl}) estimation. CV curves in the non-faradaic region of: (a) IrO_2-160; (b) IrO_2-180; (c) IrO_2-200. Current-scan rate plots of: (d) IrO_2-160; (e) IrO_2-180; (f) IrO_2-200

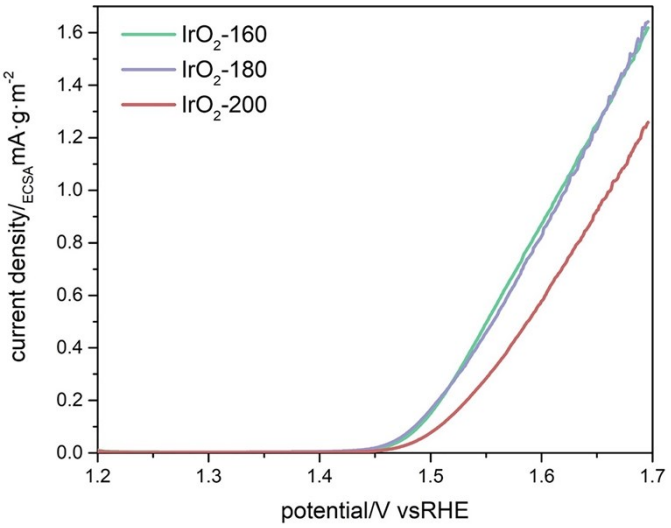

Fig. S4 LSV curves normalized by ECSA (specific activity)

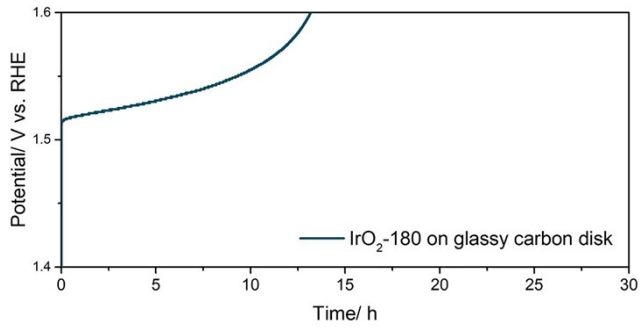

Fig. S5 CP curve of IrO_2-180 on glassy carbon disk.

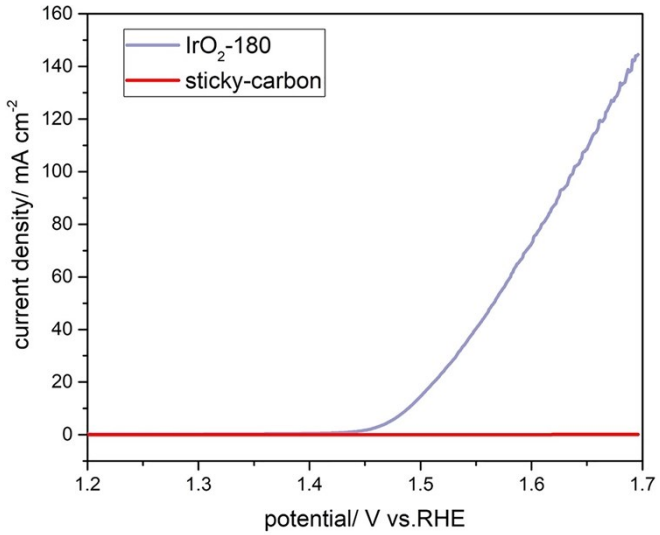

Fig. S6 LSV curves of IrO_2-180 and the bare sticky-carbon

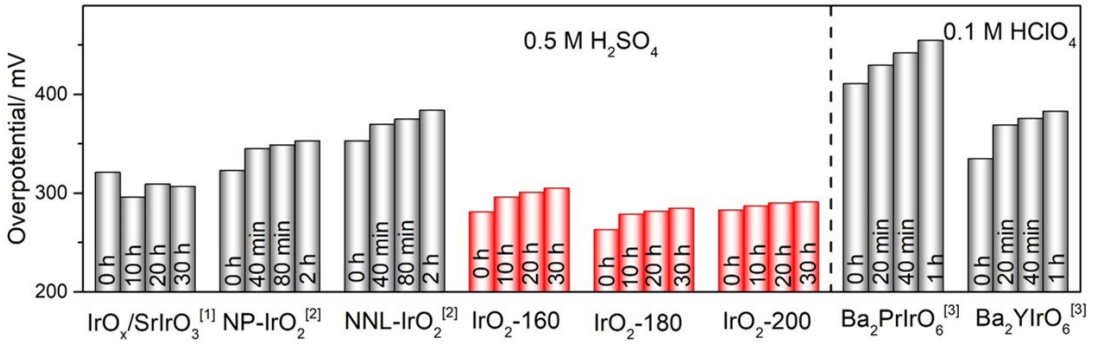

Fig. S7 (a) List of overpotentials at 10 mA·cm^{-2} current density for comparing the OER performance of IrO_2 samples obtained in this work with that of previously reported Ir-based materials

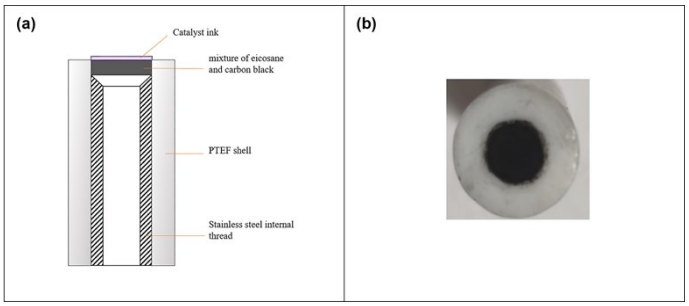

Fig. S8 The (a) Schematic diagram of internal structure and (b) actual appearance of the sticky carbon electrode.

Tables

Table. S1 Comparison of activities of the 3D hierarchical structure catalysts

Catalysts	Electrolyte	Overpotential/ mV	Tafel slope/ $mV \cdot dec^{-1}$	Mass loading/mg cm^{-2}	reference
3D NiFe-LDH	1 M KOH	229@10mA·cm^{-2}	43	0.089	[5]
3D CoMo-LDH	1 M KOH	266@10mA·cm^{-2}	49	~0.1	[6]
3D Ni–Co–P/NF	1 M KOH	270@40mA·cm^{-2}	324.6	-	[7]

Table. S2 the values of R_s and R_{ct}

Catalysts	IrO_2-160	IrO_2-180	IrO_2-200
R_s/ Ω	5.78	4.90	5.70
R_{ct}/ Ω	496.4	169.5	421.2

Table. S3 ICP-MS results of the electrolyte solution after 30-hour OER test

Catalysts	Ir in the electrolyte/ ppm	Loss mass of Ir/ %
IrO_2-160	0.0024	1.14
IrO_2-180	0.0017	0.81
IrO_2-200	0.0014	0.67

Table. S4 Comparison of ECSA with charges in synthesis conditions

Catalysts	C_{dl}/mF	ECSA/ $m^2\ g^{-1}$	Specific activity@1.6V/mA cm^{-2}
IrO_2-160	0.86	49.14	0.3344
IrO_2-180	1.54	88.00	0.3165
IrO_2-200	1.42	81.14	0.2219

Reference

1 C. C. L. McCrory, S. Jung, J. C. Peters and T. F. Jaramillo, J. Am. Chem. Soc, 2013, **135**, 16977-16987

2 P. Los, A. Lasia, H. Ménard and L. Brossard, J. Electroanal. Chem., 1993, **360** (1–2), 101–118.

3 L. Chen and A. Lasia, J. Electrochem. Soc, 1993, **140**, 2464–2473.

4 L.A. da Silva, V.A. Alves, M.A.P. da Silva, S. Trasatti and J.F.C. Boodts, Electrochimi. Acta, 1997, **42**, 271–281.

5 M. Yu, Z. Wang, J. Liu, F. Sun, P. Yang and J. Qiu, Nano Energy, 2019, **63**, 103880.

6 S. M. N. J. Nithya, J. Kim and G. Lee, Appl. Surf. Sci., 2021, **546**, 149072.

7 Y. Gong, Z. Xu, H. Pan, Y. Lin, Z. Yang and J. Wang, J. Mater. Chem. A, 2018, **6**, 12506-12514.